


Modeling the resuspension of small inertial particles in turbulent flow over a fractal-like multiscale rough surface

Ruifeng Hu ^{*}

Center for Particle-Laden Turbulence, Key Laboratory of Mechanics on Disaster and Environment in Western China, Ministry of Education, and College of Civil Engineering and Mechanics, Lanzhou University, Lanzhou 730000, China

Perry L. Johnson [†]

Department of Mechanical and Aerospace Engineering, University of California, Irvine, California 92697, USA

Charles Meneveau [‡]

Department of Mechanical Engineering, Johns Hopkins University, Baltimore, Maryland 21218, USA



(Received 28 August 2022; accepted 31 January 2023; published 13 February 2023)

Particle entrainment into a turbulent boundary layer flow is a phenomenon of great importance to many environmental and industrial processes. This paper introduces a generalized dynamic resuspension model for applicability to particles rolling on a surface with fractal-like multiscale roughness elements, which is termed the multiscale asperity model (MSAM). Furthermore, non-Gaussian (log-normal or Γ) stochastic models for the flow velocity seen by a particle are introduced and compared with a Gaussian (Ornstein-Uhlenbeck-like) stochastic model. The stochastic flow models are coupled with the MSAM and three complementary studies are performed to test their ability to predict the fraction of particles remaining on the wall after a given exposure time to turbulent flow. First, the predictions using the stochastic flow model and MSAM are compared with the experimental measurements of Reeks and Hall [*J. Aerosol Sci.* **32**, 1 (2001)]. The model predictions using the MSAM show some improvement in matching the experimental data compared with existing models, but challenges remain. Second, in order to evaluate the stochastic flow velocity models, a comparison is performed against a time-resolved direct numerical simulation (DNS) database of a turbulent channel flow coupled with the MSAM. The results show that non-Gaussianity in stochastic flow models improves the agreement with DNS-based resuspension predictions of the fraction of particles remaining on the wall after one flow through time, presumably due to more realistic probabilities of extreme flow events. Third, the prediction of particle resuspension is attempted using coarse-grained simulations (i.e., filtered DNS and large-eddy simulation for resolved flow velocity) in combination with a stochastic model for the subgrid-scale flow velocity. Comparing with (unfiltered) DNS, the simulation results confirm the importance of the inclusion of a particle subgrid-scale model to represent the effect of unresolved fluctuations on resuspension

*hur@lzu.edu.cn

†perry.johnson@uci.edu

‡meneveau@jhu.edu

dynamics. Taken together, these three tests highlight both modeling improvements and enduring challenges related to the (multifidelity) prediction of particle resuspension.

DOI: [10.1103/PhysRevFluids.8.024304](https://doi.org/10.1103/PhysRevFluids.8.024304)

I. INTRODUCTION

Particle-laden turbulent two-phase flows are ubiquitous in nature and engineering [1,2]. In many circumstances, particles are directly picked up from a solid surface by turbulent flow. For example, dust particles with diameter smaller than about $70\ \mu\text{m}$ can be entrained by strong winds into short- and long-time suspensions [3–13]. This so-called resuspension phenomenon can play an important role in sediment transport, outdoor and indoor environments, food engineering, nuclear engineering, filtration systems, etc., applications in which most surfaces are rough. Detailed background is provided in the literature [14–16].

For numerical simulation of resuspension phenomena over rough surfaces, a model is needed to describe how a particle interacts with the surface and to predict the critical condition when a particle leaves the surface. There are mainly four classes of resuspension models in the literature [15], namely, the empirical model, the static force-balance model, the kinetic probability model, and the dynamic probability model. The empirical model predicts the particle resuspension rate (ratio between particle suspension flux and surface concentration) by fitting measurement data (see, e.g., [17]). The static force-balance model gives the critical condition at which the force balance is broken [18]; however, the rolling or sliding motion of particles along a rough surface is not included. The kinetic probability model, like the model of Reeks *et al.* [19] or the Rock ‘n’ Roll model [20], can take into account the rolling motion and kinetic energy accumulation of particles on rough surfaces. This type of model requires additional phenomenological differential equations. The dynamic probability model is directly based on the fundamental principles of Newtonian mechanics to solve the rolling motion of a particle on a rough surface. For example, the stochastic dynamic model of Henry and Minier [21] divides the particle resuspension process into three steps, i.e., a particle is set into motion from a static force balance, followed by particle rolling on a surface including roughness and then a particle hitting a large asperity so it is lifted off the surface.

A key factor in particle resuspension models is to include account of surface roughness [22]. Very often the roughness length scales are small, even smaller than the viscous scales, i.e., the surface could be hydrodynamically smooth but its roughness can still greatly affect particle resuspension. We have confirmed numerically in a number of tests that a small inertial particle is very unlikely to be directly picked up by turbulent flow if placed initially on a mathematically smooth surface; thus it is crucial to account for roughness even if very small scale. In the prior dynamic model of Henry and Minier [21], a rough surface was modeled by assuming the presence of distinct small and large semispherical asperities. However, in practice, a rough surface is more likely covered by multiscale asperities [23,24]. In the present work, the resuspension model will be generalized to include a hierarchy of multiscale asperities, more closely approximating realistic surfaces.

Another important aspect for resuspension prediction is the modeling of the flow velocity seen by particles. In the dynamic stochastic model of Henry and Minier [21], the flow velocity is decomposed into its mean and fluctuating components; the latter was modeled by a Gaussian Ornstein-Uhlenbeck stochastic model using as inputs the known turbulence intensity and timescale of the fluctuating flow velocity. However, it is known that the near-wall turbulent velocity, as well as fluctuating wall-shear stress, is strongly non-Gaussian [25–27]. More specifically, it was reported that the near-wall streamwise turbulent flow velocity and wall-shear stress approximately follow a log-normal distribution [26,27]. The impact of non-Gaussianity in the flow velocity model on the prediction of particle resuspension will be assessed and discussed in the present work. While Reynolds-averaged Navier-Stokes models generally lack high fidelity and universal applicability, accurate computation of near-wall flow velocity via direct numerical simulation (DNS)

is prohibitively expensive for most practical applications. The coarse-grained simulation approach, like large-eddy simulation (LES), can provide a trade-off between cost and accuracy. In an LES, large-scale flow scales are resolved, but small scales are filtered out and need to be represented by a subgrid-scale (SGS) stress model [28–31]. To simulate particle-laden turbulent flow with the Eulerian-Lagrangian approach, a particle SGS model is also needed, without which particle dispersion would not be predicted accurately [32,33]. Numerous Langevin-type stochastic models have been developed to estimate the SGS fluid velocities in homogeneous isotropic turbulence and wall-bounded turbulence, as reviewed by Marchioli [33]. It is even more challenging to use wall-modeled large-eddy simulation where the near-wall turbulent motions are not fully resolved [34–37]. A wall model is needed to enrich the prediction of near-wall turbulent velocities and inner-outer interactions [38–44]. In this work, the effect of filtering on the particle resuspension prediction will be assessed, along with the ability of SGS stochastic models to improve LES accuracy.

The outline of the rest of the paper is as follows. Section II details the models to be used, including for particle-surface interactions and turbulent flow velocities. In particular, the multiscale asperity model is introduced to generalize the dynamic stochastic resuspension model of Henry and Minier [21] to a rough surface with multiscale asperities. Further, in addition to existing Gaussian stochastic models for fluid velocity seen by the particles, non-Gaussian models are introduced. Results from three tests are reported in Sec. III. First, model predictions are compared with the experimental measurement of Reeks and Hall [20] to demonstrate the effect of the multiscale asperity model. Second, the stochastic flow velocity models are validated by comparing their particle resuspension results with those obtained using DNS. Third, a simple stochastic particle SGS model is proposed and tested for use with coarse-grained simulations. Section IV provides a summary.

II. RESUSPENSION MODEL

For the particle resuspension criterion from a rough wall, we follow the general framework of a dynamic stochastic resuspension model of Henry and Minier [21]. In the model, the mechanics of streamwise rolling motion of a particle on a rough wall is described. A rough wall is assumed to be covered by hemispherical asperities of two distinct sizes, i.e., a large-scale one and a small-scale one. Both asperities contribute to the adhesion force acting on a particle, but only the interaction between a particle and a large-scale asperity is taken into account for the resuspension criterion. It should be noted that although the wall is covered by asperities, their sizes are much smaller than the thickness of the viscous sublayer, i.e., $D_{a,\max}^+ \ll 5$ (D_a is the asperity size and the plus superscript indicates the viscous scaling); thus the hydrodynamic smooth-wall assumption is still valid.

In this section we briefly review the models for calculating the rolling motion of a particle on such a rough wall, closely following the work of Henry and Minier [21]. A discussion of the model assumptions is provided in the Appendix. Then the two-scale asperity model is generalized to a multiscale asperity model by including a hierarchy of asperity sizes. The flow velocity model for the fluctuating or subgrid-scale flow velocity is also introduced, assuming that only the mean velocity data or the coarsely resolved fluctuating flow velocity data are available. A sketch of the physical problem considered is illustrated in Fig. 1.

A. Rolling motion of a particle on a rough surface

The equation for the rolling motion of a spherical particle along a rough surface is

$$I_p \dot{\omega}_p = M_d - M_a, \quad (1)$$

in which $I_p = \frac{7}{5} m_p R_p^2$ (m_p is the mass of the particle and R_p is the radius of the particle) is the moment of inertia of a spherical particle around a pivot point on its surface, ω_p is the angular velocity of the particle, and M_d and M_a are the aerodynamic and adhesion moments acting on the particle, respectively. The fluid-induced aerodynamic moment M_d is calculated according to

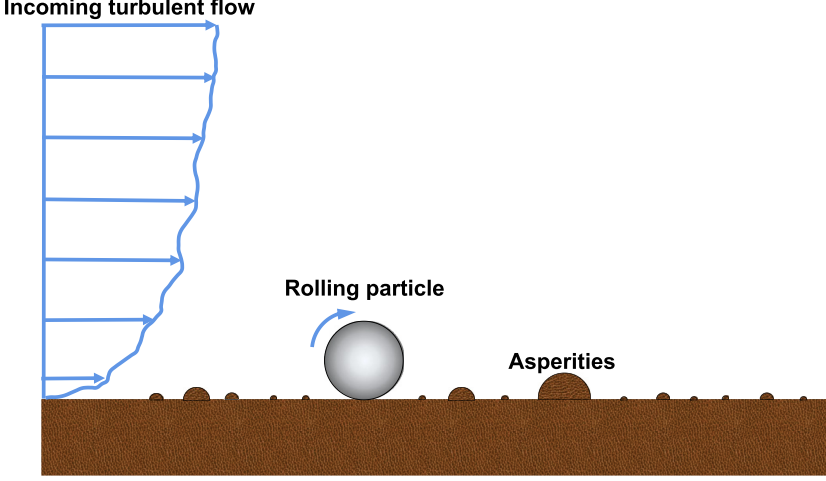


FIG. 1. Sketch of a particle rolling in a turbulent flow over a rough surface covered by fractal-like multiscale asperities. The sizes of particle and asperities are much smaller than the thickness of the viscous sublayer.

O'Neill [45] for a spherical particle moving in a linear shear flow in contact with a plane, following Henry and Minier [21].

The adhesion moment M_a is also calculated following Henry and Minier [21] by

$$M_a = F_a a_0, \quad (2)$$

in which F_a is the adhesion force acting on the particle by the rough wall and the pivot distance a_0 is defined as the relevant moment arm from the interaction between a particle and the furthest small-scale asperity in contact with the particle on its downstream side. The Derjaguin-Landau-Verwey-Overbeek (DLVO) theory [46,47] is used as the adhesion force model to calculate the van der Waals force between a particle and a rough wall, as

$$F_a = \frac{dU_a}{dz} \approx \frac{U_a(z_0 + \epsilon) - U_a(z_0)}{\epsilon}, \quad (3)$$

where $z_0 = 0.165$ nm corresponds to the constant cutoff distance, $\epsilon = 10^{-11}$ m is a infinitesimal value used to approximate the derivative, and U_a is the interaction energy between a particle and a rough wall, which is calculated by a Hamaker approach that assumes the interaction energies can be additive, i.e.,

$$U_a(h) = (1 - C_a)U_s(h) + \sum_{i=1}^{N_a} U_{i,p-a}(h), \quad (4)$$

in which U_s is the interaction energy between the particle and the smooth part of a partially rough wall, which is detailed in Ref. [48], C_a is the fraction of the surface covered by asperities, N_a is the number of asperities in contact with the particle, and U_{p-a} is the interaction energy between the particle and a hemispherical asperity, modeled by

$$U_{p-a}(h) = -\frac{A_H R_p R_a}{6h(R_p + R_a)} \left[1 - \frac{5.32h}{\lambda} \ln \left(1 + \frac{\lambda}{5.32h} \right) \right]. \quad (5)$$

Here A_H is the Hamaker constant for characterizing the van der Waals body-body interaction which depends on the particle and wall materials, λ is a characteristic wavelength for retardation effects set to 100 nm, and R_a is the radius of asperity. The values of the constants in the DLVO model,

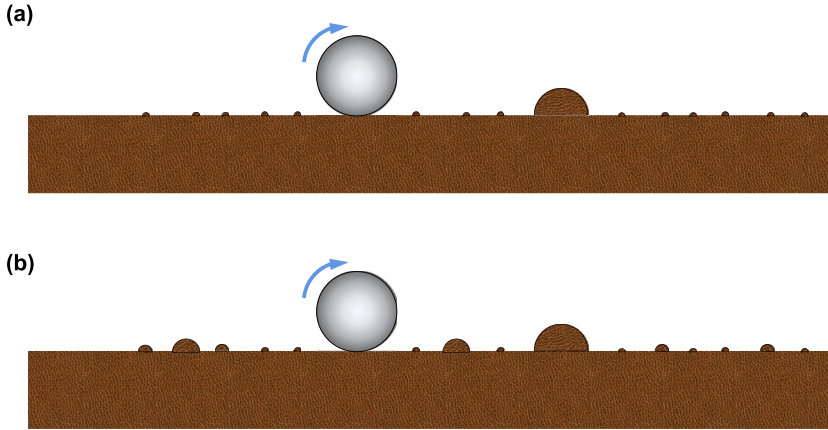


FIG. 2. Sketch of (a) the two-scale asperity model and (b) the multiscale asperity model.

i.e., z_0 , ϵ , and λ , are kept the same as in Ref. [21]. It should be mentioned that, for the airborne particles considered here, the electrostatic forces are not considered since there is no overlap between electrostatic double layers.

B. Rough-wall model and resuspension criterion

In the original dynamic stochastic resuspension model of Henry and Minier [21], a rough wall is assumed to be covered by two-level small-scale and large-scale hemispherical asperities; we refer to it as the two-scale asperity model (TSAM). The particle resuspension process is modeled by a three-stage scenario, i.e., the setting in motion of a particle (stage I), followed by its rolling motion along the rough wall due to aerodynamic and adhesion forces (stage II), and finally a detachment from the wall when a particle with sufficiently high kinetic energy collides with a large-scale asperity (stage III) (see Fig. 2). It should be stressed that no definite spatial distribution of asperities is generated in the model; instead their effects are introduced in a stochastic way. For example, the asperity number N_a in contact with a particle is stochastically generated by a Poisson distribution.

Since the introduction of distinct small-scale and large-scale asperities is somewhat arbitrary, we generalize the model by introducing a multiscale fractal-like rough wall with a hierarchy of asperity sizes [23,24]. The distribution follows $D_{n+1} = 2^{-n}D_1$, where D_n is the n th-level asperity size. Assuming a constant coverage area for different asperity sizes, the number density of asperity in each level obeys a D_n^{-2} power law, as $N(D_n) \sim D_n^{-2}$. The generalized rough surface model is referred to as the multiscale asperity model (MSAM).

In the present study, definite differentiation of large-scale and small-scale groups of multiscale asperities is still needed, the latter of which only provide adhesion action on particles while not involved in any resuspension events. We define the large-scale group of asperities responsible for resuspension as having $D_n \geq D_{\text{large}} = D_p/100$ (D_p is the particle diameter); hence the small-scale group of asperities has $D_n < D_p/100$. The sensitivity of this threshold value to the resuspension prediction is given in Sec. III A. Then if a particle hits a large-scale asperity, the resuspension criterion is whether its kinetic energy is higher than the adhesion well, i.e.,

$$E_k = m_p u_p^2 / 2 > U_a(z_0), \quad (6)$$

and if yes, the particle will be lifted off at a vertical velocity equivalent to the streamwise one before the collision (assuming elastic collision). Note that the current resuspension criterion is conceptually similar to the impulse- or work-based criterion for the incipient motion of a particle sitting on a rough bed in turbulent flow [49–51]. However, these models are for much larger particles and do not invoke the adhesion effect as it may be less important than aerodynamic forces for large particles.

Equation (6) describes the resuspension criterion used in our simulations, in which the relevant physical quantities include particle mass m_p , particle velocity u_p , and adhesion well U_a . The particle velocity is determined by Eq. (1) and the adhesion well is defined by Eq. (5). According to the above equations, we can finally find that the relevant quantities involved in the resuspension criterion are the particle density ρ_p , the particle radius R_p , the fluid density ρ_f , the fluid kinematic viscosity ν_f , the fluid friction velocity u_τ , the asperity radius R_a , and the Hamaker constant A_H . Therefore, a group of independent governing nondimensional parameters can be determined as the density ratio $\sigma = \rho_p/\rho_f$, the size ratio $\lambda = R_p/R_a$, the nondimensional particle radius $R_p^+ = u_\tau R_p/\nu_f$, and the velocity ratio u_τ/u_a , where $u_a = \sqrt{\sigma A_H/m_p}$. In addition, the particle Stokes number based on the viscous scales is defined as $St = \tau_p/\tau_f = \frac{2}{9}\sigma R_p^{+2}$, where $\tau_p = 2\rho_p R_p^2/9\rho_f \nu_f$ and $\tau_f = \nu_f/u_\tau^2$. Therefore, it can be expected that the resuspension is determined by the above nondimensional parameters or an equivalent set of recombinations.

C. Flow velocity model

The instantaneous streamwise flow velocity u_f seen by a particle is required as an input in the resuspension model. For particles having a diameter smaller than the viscous sublayer thickness $D_p^+ < 5$, the fluid velocity seen by the particle may be written as

$$u_f = \frac{\tau_w}{\mu_f} R_p. \quad (7)$$

Here τ_w is the instantaneous wall-shear stress along the wall at the location of the particle. Thus, the drag force on a particle along the wall is proportional to the local instantaneous wall-shear stress. Small-scale fluctuations of wall-shear stress are typical for turbulent flows, so accurate fluid velocities seen by particles require a direct numerical simulation on a fine mesh with a fine time step [52–54]. In contrast, it may be much more efficient and cheaper to model flow velocity by knowing mean flow velocity from a Reynolds-averaged Navier-Stokes (RANS)-like solution or coarsely resolved flow velocity from a wall-modeled LES solution.

1. Stochastic model for instantaneous flow velocity

If the mean streamwise flow velocity is known from a RANS solution or an analytical expression, we can use a stochastic model to generate an instantaneous flow velocity seen by a particle obeying several basic statistical properties of canonical wall turbulence. Henry and Minier [21] modeled the instantaneous flow velocity seen by a particle using an Ornstein-Uhlenbeck-type stochastic model, which is Gaussian in nature and written as

$$du_f^+ = -\frac{u_f^+ - U_f^+}{T^+} dt + \sqrt{\frac{2}{T^+}} \sigma_{u_f^+} dW^+, \quad (8)$$

where u_f^+ is instantaneous streamwise flow velocity seen by a particle, $U_f^+ = \langle u_f^+ \rangle$ is the mean streamwise flow velocity ($\langle \cdot \rangle$ is the average operator), T^+ is the correlation timescale of the flow (which is set to 40 according to Ref. [21] if not explicitly noted), $\sigma_{u_f^+}$ is root-mean-squared (rms) value of u_f^+ , dt is the time step, and dW^+ is a discrete Wiener process. Here the plus superscript indicates the viscous normalization by ν_f (the fluid kinematic viscosity) and the friction velocity u_τ ($u_\tau = \sqrt{\langle \tau_w \rangle}/\rho_f$, where $\langle \tau_w \rangle$ is the mean wall-shear stress).

The particle size considered in this work is much less than the thickness of the viscous sublayer, and the dispersed phase is so dilute that one-way coupling is appropriate (neglecting the feedback of particles to fluid flow). Therefore, the mean streamwise flow velocity can be modeled by the linear law [29], as

$$U_f^+ = R_p^+, \quad (9)$$

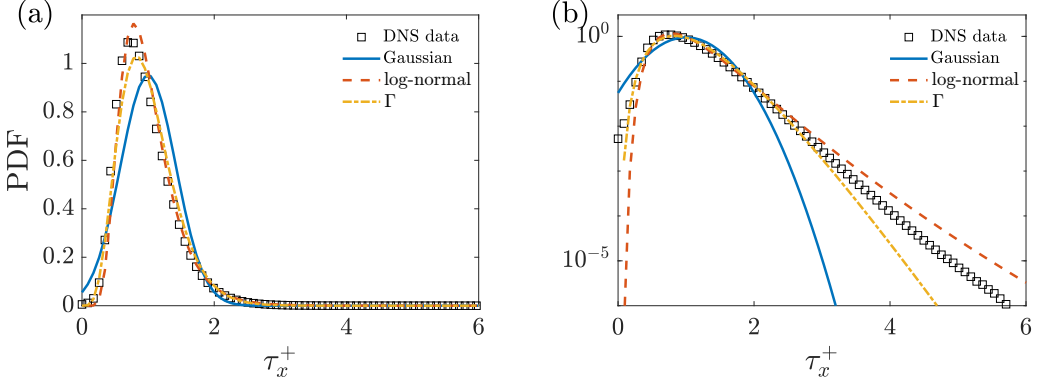


FIG. 3. Probability density function of the streamwise wall-shear stress from the DNS data, as well as the Gaussian and non-Gaussian (log-normal or Γ) PDFs.

and the rms value of the fluctuating flow velocity is modeled by an empirical fitting formula [55], as

$$\sigma_{u_f}^+ = \frac{0.4R_p^+}{1 + 0.00239R_p^{+1.496}}. \quad (10)$$

On the other hand, it has been well documented that the statistics of near-wall turbulence velocities and wall-shear stress are not Gaussian [25–27,54,56]. Figure 3 shows the probability density function (PDF) of streamwise wall-shear stress from a channel DNS database at $\text{Re}_\tau = 1000$ [57], together with the Gaussian and the non-Gaussian (log-normal or Γ) PDFs. The parameters in the PDF expressions, i.e., the mean wall-shear stress $\langle \tau_{w,x} \rangle$ and its rms value $\sigma_{\tau_{w,x}}$, are directly obtained from the DNS data. It should be noted that only $\tau_{w,x} > 0$ data are used, and the negative wall-shear events (which are very infrequent) are not taken into account, because only positive flow velocity is used in the resuspension model. It is expected that rare instances of negative velocities do not significantly impact particle resuspension behavior.

Figure 3(a) displays the PDFs in linear coordinates. It can be seen that the log-normal distribution and the Γ distribution are in much better agreement with the DNS data than the Gaussian distribution. On the other hand, Fig. 3(b) plots the PDFs on a semilogarithmic scale to examine the relative probability of extreme wall-shear stress events. The probability of $\tau_{w,x}^+ > 2$ is evidently underestimated by the Gaussian distribution, but only slightly overestimated by the log-normal model and slightly underestimated by the Γ model. Therefore, the wall-shear stress is highly non-Gaussian, and the log-normal model or the Γ model can be expected to give a better prediction of the probability of encountering extreme events than the Gaussian model.

Thus, we aim to model the fluid velocity seen by particles considering the non-Gaussianity of flow velocity [29]. We employ a log-normal or a Γ stochastic model which provides improved predictions of the PDF of wall-shear stress or near-wall velocity especially for infrequent large-magnitude events. The log-normal model is [29]

$$dY^+ = -\frac{Y^+ - \mu_L^+}{T^+} dt + \sqrt{\frac{2}{T^+}} \sigma_L^+ dW^+, \quad (11)$$

in which

$$Y^+ = \ln u_f^+, \quad \mu_L^+ = \ln(U_f^{+2}/\sqrt{U_f^{+2} + \sigma_{u_f}^{+2}}), \quad \sigma_L^+ = \sqrt{\ln(\sigma_{u_f}^{+2}/U_f^{+2} + 1)}. \quad (12)$$

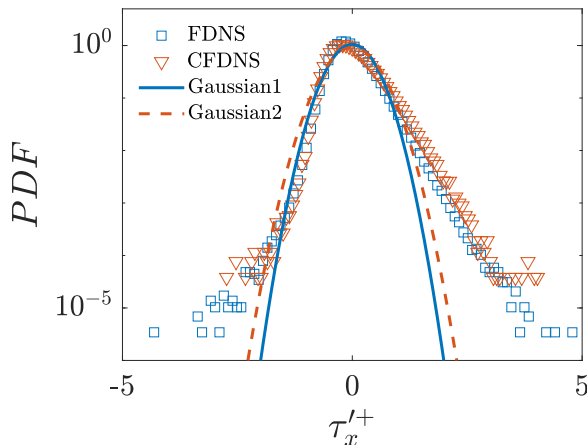


FIG. 4. Probability density functions of the subgrid scale streamwise fluctuating wall-shear stress with a filter (FDNS) and a coarser filter (CFDNS). Gaussian1 and Gaussian2 are the corresponding Gaussian PDFs to FDNS and CFDNS, respectively.

The Γ model can be written as [29]

$$du_f^+ = -\frac{u_f^+ - U_f^+}{T^+} dt + \sqrt{\frac{2U_f^+ u_f^+}{T^+}} \sigma_{u_f^+}^+ dW^+. \quad (13)$$

The models (9) and (10) for the mean flow velocity U_f^+ and the rms value of fluctuating flow velocity $\sigma_{u_f^+}^+$ are still adopted in the non-Gaussian stochastic models (11) and (13).

2. Stochastic model for subgrid-scale flow velocity

In a coarse-grained simulation, e.g., large-eddy simulation, only a resolved flow velocity \tilde{u}_f above the filter length scale is provided, and the omission of a subgrid-scale (SGS) flow velocity $u'_f = u_f - \tilde{u}_f$ will typically cause biased predictions of particle resuspension [33]. Figure 4 shows PDFs of streamwise subgrid-scale wall-shear stress from the channel DNS database using two planar box filters in the two wall parallel directions. The first filtering width is chosen as 16 times the DNS grid size (i.e., $\Delta_x^+ = 196$), the same as that used in Ref. [58], while the second filter scale is twice coarser. It is seen that the subgrid-scale wall-shear stress is also non-Gaussian. However, implementation of a non-Gaussian model of the type used for the RANS-level modeling described in the preceding section is challenging. The SGS stress fluctuations exhibit both positive and negative values while the log-normal and Γ distribution models represent only positive fluctuations. Also, in filtered DNS, we have verified that some asymmetry (non-Gaussianity of the large-scale stress fluctuations) is present at the filtered level. Thus, for the present purposes, a simple Gaussian Ornstein-Uhlenbeck-type stochastic SGS flow velocity model will be used to approximate the flow velocity seen by a particle in coarse-grained simulation. While not accounting for non-Gaussianity at the SGS scales, such a model allows for testing the basic effect of SGS fluctuations on particle resuspension. Development of non-Gaussian wall-shear stress SGS models is left for future efforts.

The present stochastic model for SGS wall-shear stress is based on the Gaussian Ornstein-Uhlenbeck-type process, i.e.,

$$du_f^+ = -\frac{u_f^+}{T^+} dt + \sqrt{\frac{2}{T^+}} \sigma_{u_f^+}^+ dW^+. \quad (14)$$

Here $\sigma_{u_f}^+$ is the rms value of the SGS flow velocity u_f^+ , which can be estimated using DNS data as

$$\sigma_{u_f}^{+2} = \sigma_{u_f}^{+2} - \sigma_{\tilde{u}_f}^{+2}, \quad (15)$$

where $\sigma_{\tilde{u}_f}^+$ is the rms value of the resolved flow velocity \tilde{u}_f , which was actually obtained from wall-shear stress data and using (7). We found from the data that the relation (15) is a good approximation, since the resolved and the SGS wall-shear stresses are approximately uncorrelated. Note that the specific values used in the present application are tuned specifically from filtered DNS data and thus lack generality. The approach is followed for demonstration purposes and for motivating future work to develop more general models.

III. RESULTS

A. Comparison with experimental measurement

First, we compare the model predicted Φ_{mod} (remaining particle fraction) on a wall after 1 s exposure to airflow with experimental data of Reeks and Hall [20]. The measurement is conducted in a long duct with a rectangular section. In the experiment, the duct is horizontally placed (normal to gravity). The height of the duct is 0.02 m and the width is ten times larger, so it can be approximately regarded as a plane channel flow with a half height of $H = 0.01$ m. The test section is 3.5 m downstream along the duct, where the flow is fully developed. The friction velocities in the experiment range between approximately 0.2 and 5.0 m/s. Therefore, we can estimate that the friction Reynolds number is roughly in the range $\text{Re}_\tau \approx 130\text{--}3300$ with air viscosity $\nu_f = 1.57 \times 10^{-5}$ m² and air density $\rho_f = 1.3$ kg/m³, which is well within the fully turbulent regime of channel flow [59–62].

For the model, 10 000 particles are initialized on the wall at rest with a uniformly random planar distribution. The densities of the alumina and graphite particles are 1600 and 2300 kg/m³, respectively. The time step in the simulation is set to 10^{-6} s, which is small enough to produce accurate and statistically converged results. The model and physical parameters in the simulations are kept the same as in [21] and can be found there. It should be noted that we use a total surface coverage of asperities $C_a = 6\%$ in the present stochastic simulations (0.6% for each hierarchy of asperities), the same as in [21]; the exact value was absent in the experimental measurement of Reeks and Hall [20]. The size distribution of asperities was also not measured and reported. For the MSAM simulation, the minimum and maximum asperity radii are 5 nm and 2 μm , respectively, and the number of asperity levels is set to 10. As the overall model output we consider the fraction of particles that remain on the wall after 1 s, denoted by Φ_{mod} . Stronger resuspension will correspond to smaller Φ_{mod} and vice versa. Results are obtained for various values of the velocity ratio u_τ/u_a .

We performed simulations using the TSAM and MSAM coupled with the Gaussian stochastic flow velocity models with the mean flow velocity according to Eq. (9). The results are compared with the experimental results of Reeks and Hall [20] in Fig. 5. In addition, the simulation results of the three different particles (different material or/and size) in Reeks and Hall's experiment are also displayed in Figs. 5(a), 5(b), and 5(c), respectively. The reference velocity u_a is solely determined by the particle and fluid properties and unchanged for each kind of particle. In each plot we only varied the value of u_τ to obtain the given data points. It can be seen that the predictions for the fraction of remaining of particles on the wall using the MSAM vary less steeply with respect to a normalized friction velocity than those by the TSAM, and the former are often in better agreement with the experimental data, but not always so. In addition, the predictions using the MSAM at small friction velocity are generally good, but the predictions at high wind velocity are all underestimated, which may be attributed to physics that is not considered by the model, e.g., the wind velocity deficit in the wake of asperities and particles (the sheltering effect) or the effect of particle collision [63].

Furthermore, we assess the sensitivity of the resuspension prediction to the threshold size of large-scale asperities D_{large} and the results are displayed in Figs. 5(d)–5(f). Besides $D_{\text{large}} = D_p/100$, another two threshold sizes of $D_{\text{large}} = D_p/50$ and $D_p/200$ are chosen for comparison. It can be seen that the prediction results have a notable sensitivity to D_{large} , and using $D_{\text{large}} = D_p/100$ generally

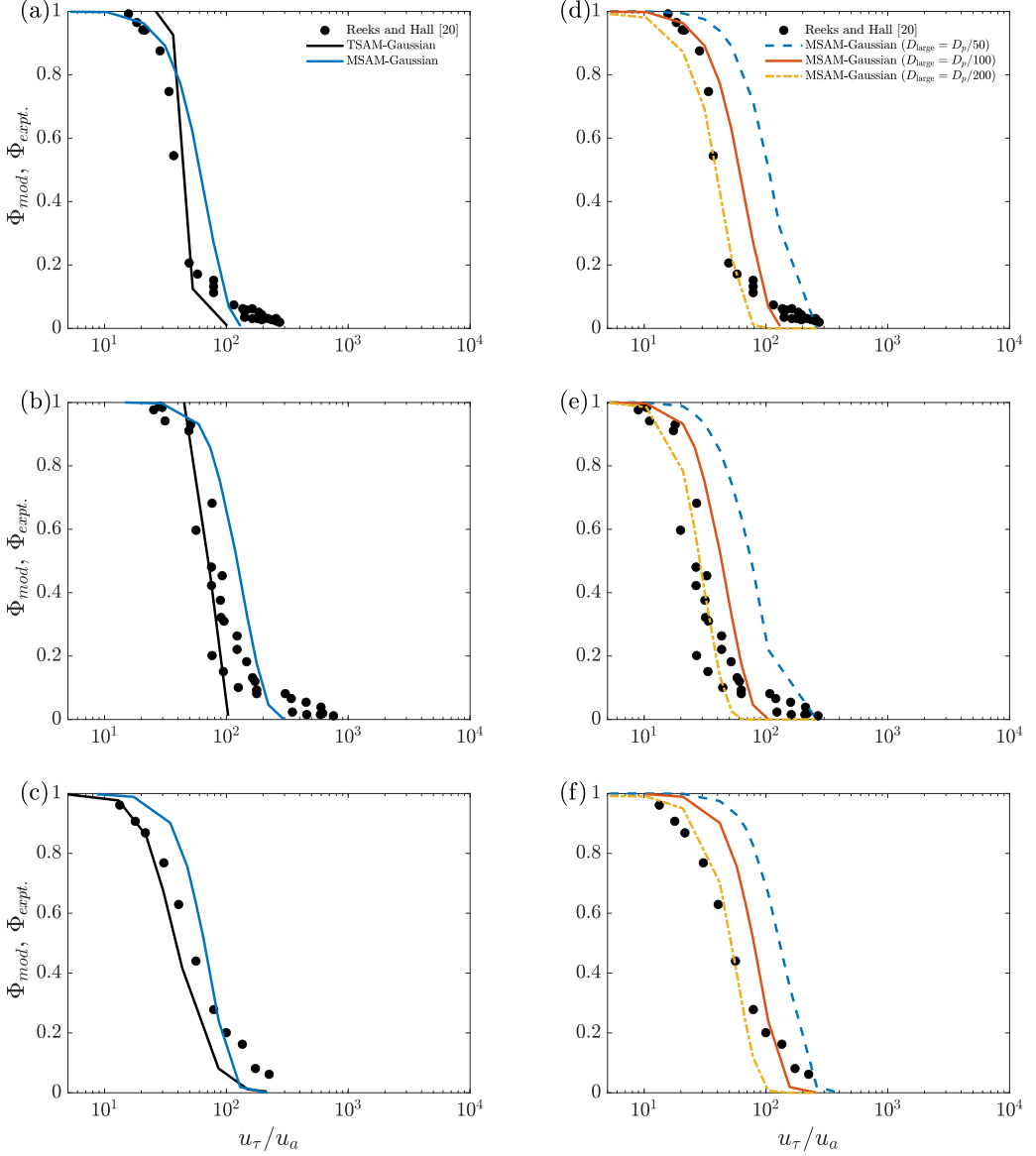


FIG. 5. Fraction of particles remaining on the wall after 1 s exposure to airflow with varying wind friction velocity u_τ . Here $u_a = \sqrt{\sigma A_H/m_p}$ is a reference velocity scale, $\sigma = \rho_p/\rho_f$ is the density ratio, A_H is the Hamaker constant, and m_p is the mass of the particles. The particle parameters are (a) and (d) alumina particles with $R_p = 5 \mu\text{m}$, (b) and (e) alumina particles with $R_p = 10 \mu\text{m}$, and (c) and (f) graphite particles with $R_p = 6.5 \mu\text{m}$. The Hamaker constant is set to 25×10^{-20} J for alumina particles and 80×10^{-20} J for graphite particles, the same as in [21]. The minimum and maximum asperity radii are 5 nm and $2 \mu\text{m}$, respectively, and the number of asperity levels is set to 10. The total asperity coverage is 6% (0.6% for each hierarchy of asperities). (d)–(f) Sensitivities of remaining fraction of particles with the threshold size of large-scale asperities.

yields better predictions of the remaining particle fraction, which validates the present choice of $D_{\text{large}} = D_p/100$. However, we should emphasize that the sensitivity of resuspension prediction to the threshold is not small and D_{large} can be regarded as an additional free parameter in the model.

Therefore, it provides more flexibility for the resuspension prediction by the MSAM compared with the TSAM.

B. Validation of the stochastic flow velocity model

In order to accurately quantify the effects of the stochastic flow velocity models, i.e., Eqs. (8), (11), and (13), we resort to using DNS of turbulent flow and simulate particle resuspension with the MSAM as reference data. Other model components are kept fixed to isolate the effect of the flow velocity model. More specifically, we use the turbulent channel flow data set at $Re_\tau = 1000$ available from Johns Hopkins Turbulence Databases [57] as the background flow to compute the particle motion in one-way coupling. The channel flow data set is produced by a DNS in a wall-normal velocity-vorticity form using a pseudospectral method in the horizontal plane and a seventh-order B -spline collocation method in the wall-normal direction [64]. Dealiasing is performed using the $3/2$ rule. Temporal integration is performed using a low-storage third-order Runge-Kutta method. The simulation domain size is $8\pi \times 2 \times 3\pi$ with a spatial resolution of $2048 \times 512 \times 1536$ in the streamwise (x), wall-normal (y), and spanwise (z) directions, respectively. The grid resolution of the DNS data is relatively standard, i.e., $\Delta x^+ \approx 12$ and $\Delta z^+ \approx 6$. The effect of grid resolution on wall-shear stress fluctuations has been investigated in detail by Yang *et al.* [54]. These authors observed that the standard grid resolution resolves about 99% of the wall-shear stress fluctuations at $Re_\tau = 180$. Further, that paper estimated that only a slightly higher resolution is necessary at $Re_\tau = 5200$ to capture 99% of the fluctuations. Of course, some very rare events will be obscured by the grid resolution, but this has a minimal impact on our results here. The error of the log-normal or Γ models in precisely reproducing the PDF is much more significant than the relatively small error observed by Yang *et al.* [54]. In total, 4000 snapshots in a flow through time approximately ($L_t \approx 26$) are available in the database. The three velocity components and pressure data are stored every five time steps, corresponding to a nondimensional database time step $\Delta t = 0.0065$ (normalized by the bulk velocity and half channel height). Initially, 10 000 particles are put on the wall at rest with a uniformly random planar distribution.

In this work we only compute the rolling motion and the resuspension of a particle on a rough surface, while not taking into account wall interactions of particles that have already been entrained in the bulk of the flow. The particle size considered here is much smaller than the thickness of the viscous sublayer; therefore, we use the instantaneous streamwise wall-shear stress $\tau_{w,x}$ from the DNS data and the linear law to give the instantaneous flow velocity seen by a particle, i.e., Eq. (7). Three kinds of particles, namely, the same as those in the experiment of Reeks and Hall [20], are considered. Specifically, we consider alumina particles with $R_p = 5 \mu\text{m}$, alumina particles with $R_p = 10 \mu\text{m}$, and graphite particles with $R_p = 6.5 \mu\text{m}$. The air density is 1.3 kg/m^3 and the density ratios of the alumina and graphite particles to air are 1230 and 1770, respectively. The Stokes number St defined by viscous scales is on the order of $1-10^3$ in our simulations. The Hamaker constants for the alumina and graphite particles are 25×10^{-20} and 80×10^{-20} J, respectively. The total surface coverage of asperities is 10% (1% for each hierarchy of asperities).

Since the DNS provides a convenient common reference, we compare the model predictions using the Gaussian and non-Gaussian flow velocity models with known mean velocity, i.e., Eqs. (8), (11), and (13), to the results obtained using the known DNS velocity. Results are shown in Figs. 6(a)–6(c). It can be seen that the Gaussian model yields an overprediction of the fraction of particles remaining at the surface or an underprediction of the resuspension rate. This is probably owing to the underprediction of extreme flow velocity events generated by the Gaussian model, which are rare but may play an evident role in particle resuspension. On the other hand, the non-Gaussian models yield predictions in better agreement with the DNS results, further supporting that the non-Gaussianity of the near-wall velocity is an important factor in particle resuspension. To further quantify the difference between the predictions using the stochastic flow velocity models and DNS flow data, we show their fraction difference $\Phi_{\text{mod}} - \Phi_{\text{DNS}}$ in Figs. 6(d)–6(f). It can be seen that for the three types of particles, the maximum fraction difference with the Gaussian model can

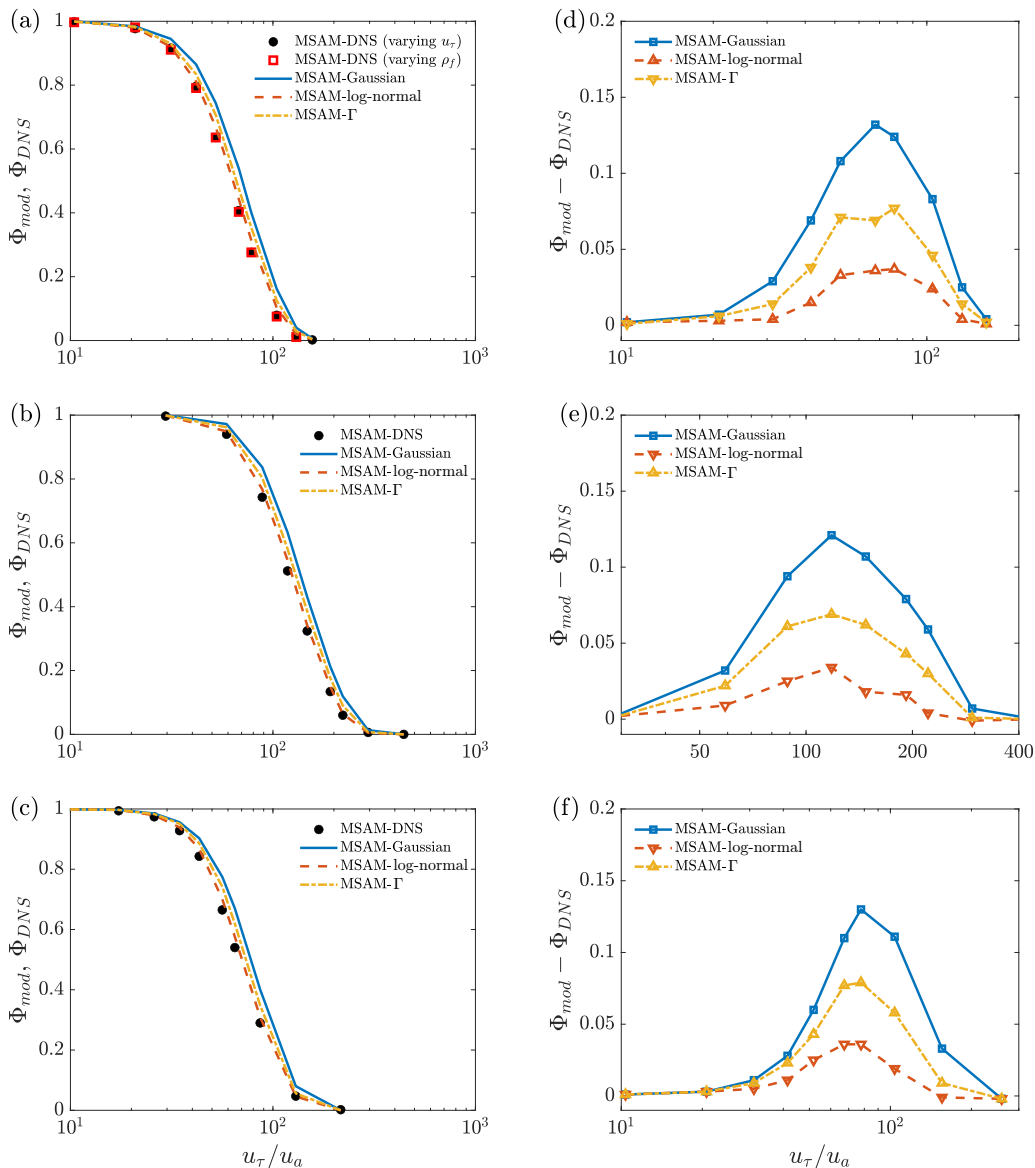


FIG. 6. (a)–(c) Fraction of particles remaining on the wall after a time exposure of one flowthrough to flow with varying velocity ratio u_τ/u_a using the channel DNS data for the three particles as in Fig. 5.

exceed 10% and that the difference (error) when using the log-normal model is about 3 times smaller than when using the Gaussian model. It can also be seen that there is a maximum in the error for an intermediate u_τ/u_a . This is qualitatively explained as follows. At very small friction velocity, all of the particles remain attached on the wall and this is easy to predict. At very large friction velocity, all of the particles are removed from the surface; again, this is easy to predict. At intermediate friction velocity, a significant portion of particles are removed while another significant proportion remain attached. In this regime, the predicted resuspension rate is most sensitive to the modeling error, so a maximum error occurs near the friction velocity where roughly half of the particles remain attached. Furthermore, Secs. III A and III B together show that the stochastic flow velocity model has some

influence on the prediction and non-Gaussianity does improve agreement with the DNS, but it is generally smaller than other concerns such as how to model the particle-roughness interactions.

Note also that the DNS data are nondimensional and need to be transformed into dimensional data if applied to an actual particle resuspension problem. A question is whether u_τ/u_a uniquely determines the resuspension rate at a fixed flow Reynolds number and particle-to-fluid density ratio. For this purpose, we consider two variations, by varying the friction velocity u_τ while keeping others unchanged or varying ρ_f and ρ_p while keeping others unchanged. In these transformations, the three aforementioned similarities are satisfied, i.e., the particle-to-fluid density ratio similarity (σ), the particle-to-asperity size ratio similarity (λ), and the velocity ratio similarity (u_τ/u_a), while the viscous-scaled particle size R_p^+ is different. Figure 6(a) shows the results using the different transformations. It can be seen that the remaining fraction Φ_{mod} after one flowthrough time is exactly the same by the two transforms, validating the similarity of the velocity ratio u_τ/u_a .

C. Coarse-grained simulation with stochastic subgrid-scale flow velocity model

In this third and final test, *a priori* and *a posteriori* testing is performed for wall-modeled LES predictions of particle resuspension, with and without a stochastic model for the unresolved fluctuations. For coarse-grained simulation for turbulent flow, we first perform filtering of the DNS data in both time and space, i.e., filtered DNS (FDNS), to mimic an ideal large-eddy simulation. A two-dimensional box filter is used to calculate the filtered wall-shear stress at the wall with two resolutions. The first one is the same as that in Ref. [58], where all 16 wall-shear stress snapshots were downloaded and filtered in space with a box filter 16 times larger than the DNS resolution ($\Delta x^+ \approx 196$ and $\Delta z^+ \approx 98$). The second resolution is twice coarser, so it is 32 times the DNS resolution in time and space ($\Delta x^+ \approx 392$ and $\Delta z^+ \approx 196$). Figure 7 shows the remaining fraction of particles using FDNS data with or without the subgrid-scale flow velocity model, i.e., Eq. (14). It is seen from Fig. 7 that the FDNS without SGS flow velocity model (MSAM FDNS) significantly overestimates the fraction of particles remaining or underestimates the resuspension rate. The coarser FDNS (MSAM CFDNS) slightly increases the overestimation of the remaining fraction or the underestimation of the resuspension rate. The maximum fraction difference with the DNS results can reach 30%–40%. On the other hand, by including the SGS flow velocity with Gaussian distribution, i.e., the model (14), the prediction for the remaining fraction is much improved. The maximum fraction difference is reduced to about 10%, which is consistent with the results in Fig. 6. The effect of different filter widths seems to be only marginal. Therefore, the results presented here indicate the necessity of adding an SGS flow velocity component in predicting the resuspension of particles.

In order to test the proposed resuspension model in the context of a realistic coarse-grained simulation (*a posteriori* testing), we follow the approach of Ref. [58] and perform large-eddy simulation of channel flow at $\text{Re}_\tau = 1000$ and couple the coarse-grained flow fields with the stochastic SGS flow model. The open source LESGO code [65] was employed to simulate the channel flow with a series of snapshots that match those from the FDNS data. The code uses a pseudospectral treatment with 2/3 dealiasing in the wall-parallel directions and second-order finite differencing on a staggered grid in the wall-normal direction. The second-order Adams-Bashforth scheme is used for time advancement, and the pressure Poisson equation is solved to satisfy the divergence-free condition on the velocity field. The scale-dependent dynamic Smagorinsky model [66,67] is adopted for the SGS stress closure. The equilibrium wall model [68] is implemented as the first off-wall grid lying in the logarithmic region. The computation domain size is the same as the DNS one, i.e., $8\pi \times 2 \times 3\pi$ in the x , y , and z directions. Two grids are generated, namely, a normal one with $128 \times 32 \times 96$ and a coarser one with $64 \times 16 \times 48$. Note that the grid in the wall-normal direction is uniformly distributed.

Figure 8 shows the remaining fraction of particles Φ_{LES} using the LES solution with or without a subgrid-scale flow velocity model. The results are quite similar with the FDNS. The LES without SGS flow velocity model (MSAM LES) significantly overestimates the fraction of particles remain-

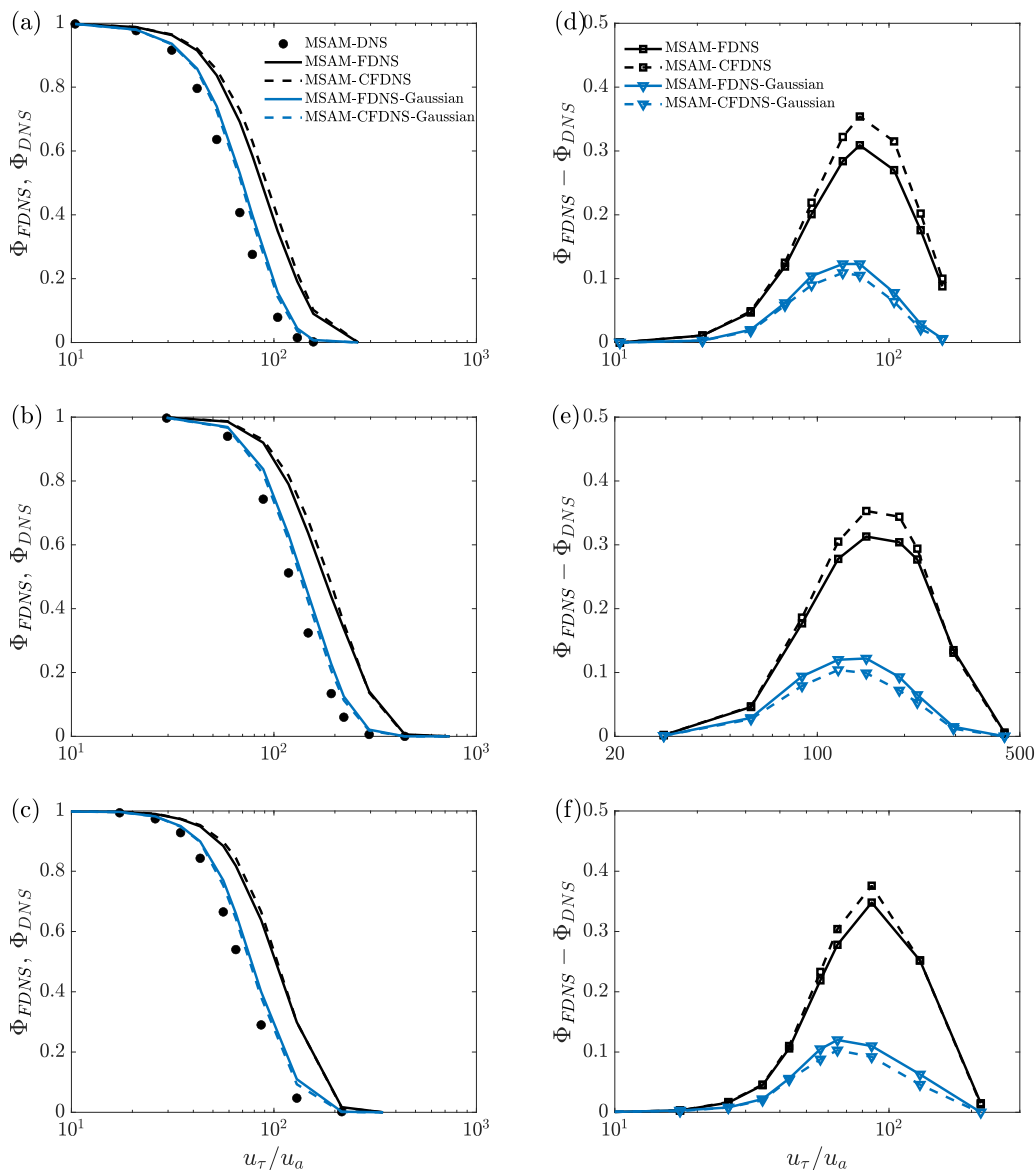


FIG. 7. (a)–(c) Fraction of particles remaining on the wall after a time exposure of one flowthrough to flow for the three particles as in Fig. 6. The total asperity coverage is 1%. (d)–(f) Fraction difference between the predictions using filtered DNS and DNS flow data.

ing or underestimates the resuspension rate. The coarser LES (MSAM CLES) slightly increases the overestimation of the remaining fraction or the underestimation of the resuspension rate. In addition, by including the SGS flow velocity with the Gaussian distribution, i.e., the model (14), the prediction for the remaining fraction is much improved. The maximum fraction difference is reduced to about 10%. The effect of different filter widths seems to be only marginal. Note that the SGS model was tuned using knowledge of the wall-shear stress variance from DNS. This enabled the current demonstration of the importance of the SGS model. For general applicability, the model must be supplied with additional modeling needed to prescribe the SGS wall stress fluctuation variance. Future work is needed in this regard.

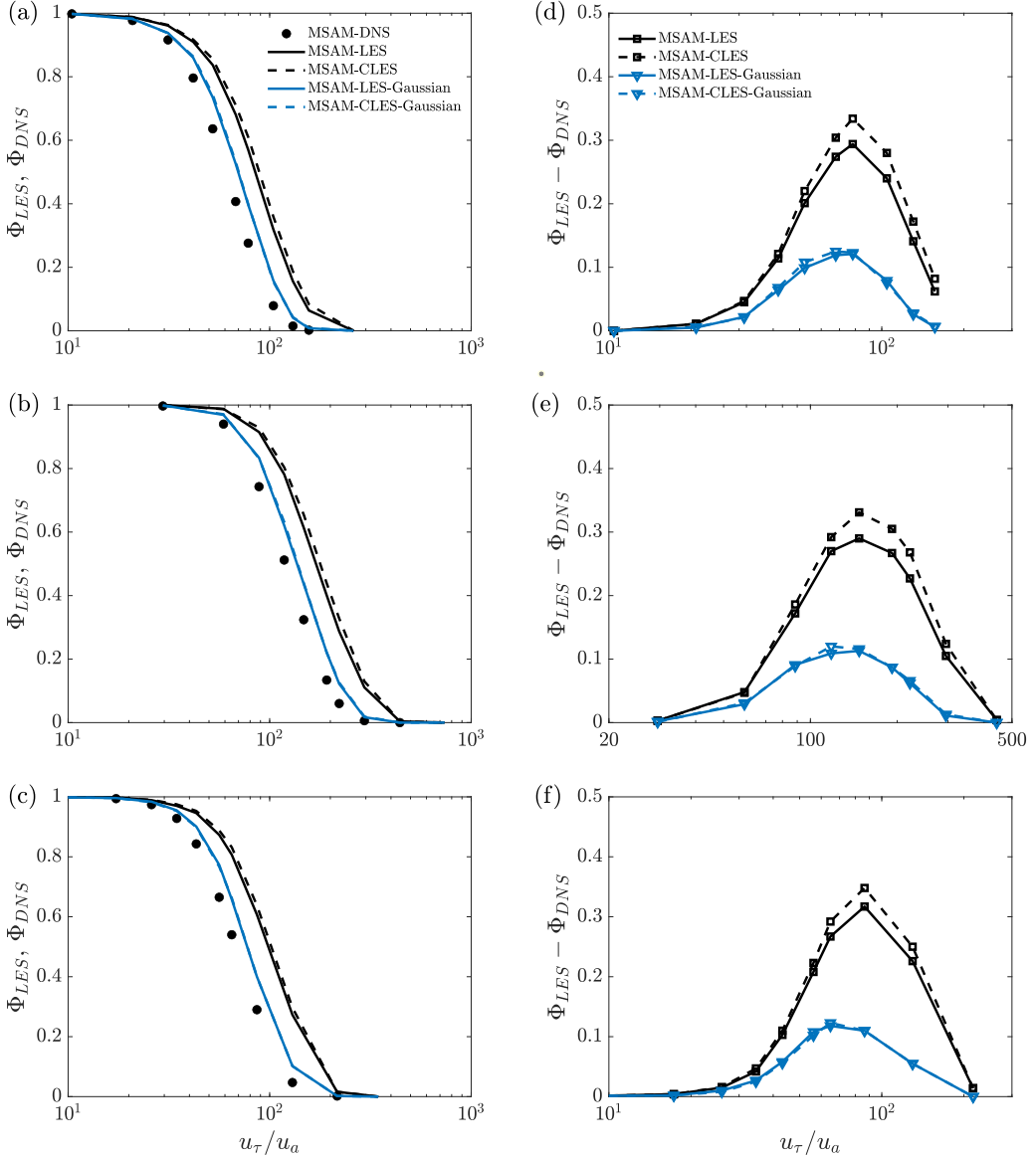


FIG. 8. (a)–(c) Fraction of particles remaining on the wall after a time exposure of one flowthrough to flow for the three particles as in Fig. 6. The total asperity coverage is 1%. (d)–(f) Fraction difference between the predictions using LES and DNS flow data.

Finally, we would like to clarify the difference between the results of Secs. III C and III B. In Sec. III B we dealt with the stochastic model for the total fluctuating velocity containing all scales of turbulent motions, and the mean flow velocity is given like a RANS solution. In this circumstance, we found that the non-Gaussianity of fluctuating flow velocity plays a visible but not vital role. On the other hand, in Sec. III C, coarse-grained simulation (filtered DNS or LES) can provide large-scale-resolved flow velocity containing a large portion of turbulent motions, while small-scale unresolved motions are modeled by the stochastic SGS flow velocity model. Although the SGS flow velocity is non-Gaussian as shown in Fig. 4, it is not as straightforward to model by

a stochastic process. We found that a Gaussian stochastic SGS flow velocity model can account for most of the error by ignoring the SGS flow velocity, and including non-Gaussianity may be expected to provide only a small additional improvement.

IV. CONCLUSION

In this study we numerically solved the equations of particle motion with a resuspension model to simulate the resuspension of small inertial particles by a wall-bounded turbulent flow. The resuspension model of Henry and Minier [21] was generalized to a more realistic multiscale rough surface geometry that often improves agreement with the experimental data. To isolate the effect of the fluid velocity stochastic model, the multiscale asperity resuspension model was coupled with a time-resolved DNS database of channel flow for comparison while keeping the asperity model fixed. It was found that a log-normal stochastic model for the instantaneous flow velocity can generate a more accurate prediction of particle resuspension than the Gaussian stochastic model; however, the error attributable to the flow velocity model is small compared to other aspects of the resuspension model. Finally, we coupled the resuspension model with coarsely grained simulation, i.e., filtered DNS and LES, as well as a Gaussian stochastic model for the SGS flow velocity. It was shown that LES without an SGS velocity fluctuation model causes significant errors (underestimation) in the resuspension prediction compared with DNS and the inclusion of the SGS model significantly improves the prediction.

Further refinements of the resuspension modeling introduced here can be considered. For example, one could develop and include a non-Gaussian SGS flow velocity model. Also, one may consider possible sheltering effects in the asperity model as well as the effects of particle collision [63]. The results here provide an important step toward developing a more complete large-eddy simulation framework to predict particle resuspension processes with high accuracy [69]. Wall models that incorporate the inner-outer interaction physics [38–44] may also be important to such efforts.

ACKNOWLEDGMENTS

R.H. acknowledges financial support from the National Natural Science Foundation of China (Grants No. 11972175 and No. 92052202) and the China Scholarship Council. The authors would like to thank C. Henry, J. P. Minier, and S. Chibbaro for helpful communications.

The authors report no conflict of interest.

APPENDIX: MODEL ASSUMPTIONS

In this Appendix we would like to discuss and justify the underlying assumptions in modeling particle motion of this work, i.e., the ignorance of slipping motion, gravity, lift, lubrication, and particle-particle and particle-flow interactions.

(i) *Possible slipping motion.* Slipping motion is possible if the aerodynamic force on particle is larger than the friction force. We have checked that the aerodynamic force is about two to three orders of magnitude smaller than the van der Waals adhesion force (in the wall normal towards the surface) on average and it is probably also smaller than the friction force as the friction coefficient is commonly on the order of 10^{-1} –1 (e.g., 1.05 for aluminum on aluminum). Therefore, it is reasonable to only consider purely rolling motion in our simulations and there is no need to solve the linear momentum equation of particle motion.

(ii) *Gravity and lift.* We have checked that the gravity is two to four orders of magnitude smaller than the adhesion force on average, so it can be reasonably neglected. Recently, Bragg *et al.* [70] showed that gravitational settling may play a role in determining particle concentration and velocity distribution in a particle-laden wall-bounded turbulent flow. In their work, particles were introduced at the upper plane of the domain and settled down under gravity and turbulence, which is different

from the present resuspension setup. Here we just consider purely rolling motion of particles on the horizontal wall, so only horizontal aerodynamic and adhesion moments are considered. In other words, we did not compute particle motion away from the wall and into the fluid flow; thus the gravitational settling is not included. We have also checked that the Saffman lift is smaller than the gravity on average, so the lift force is also neglected and a small heavy particle considered here is unable to be directly picked up away from the wall by the aerodynamic lift alone.

(iii) *Lubrication*. Lubrication force is generated by relative motion between two surfaces getting very close, when the fluid between the gap is squeezed out. There have been several analytical models for calculating the lubrication force and torque in the Stokes regime [71–73]. In the wall-normal direction, the normal lubrication force is infinite if a particle is in contact with a smooth surface. Usually a minimum height related to surface roughness size is prescribed in computations, and the normal lubrication force is assumed to be zero or continuously varied when the gap size is smaller than the minimum height [74–83]. Nevertheless, the normal lubrication force is proportional to the normal relative velocity between the two surfaces. In our case, particles are rolling along a surface and there is no normal relative motion between the particle and the surface; thus the normal lubrication force can be neglected. For the tangential lubrication force and torque, analytical models have also been developed [84,76,81], in which it is assumed that the tangential lubrication force and torque are zero for surfaces that are in contact with each other. Therefore, the tangential lubrication force and torque are also neglected. However, the lubrication force would presumably resist the particle as it leaves the surface, which is potentially a topic for further study in the future, as we only focus on particle rolling motion on the wall in this work.

(iv) *Particle-particle and particle-flow interactions*. In our simulations, the initial particle volume fraction (in a slab with a height of particle diameter) is on the order of 10^{-11} – 10^{-6} ; thus it is well within the one-way coupling regime [1,85] and particle-particle (four-way coupling) and particle-flow (two-way coupling) interactions can be omitted.

-
- [1] S. Balachandar and J. K. Eaton, Turbulent dispersed multiphase flow, *Annu. Rev. Fluid Mech.* **42**, 111 (2010).
 - [2] L. Brandt and F. Coletti, Particle-laden turbulence: Progress and perspectives, *Annu. Rev. Fluid Mech.* **54**, 159 (2022).
 - [3] G. A. Bagnold, *The Physics of Blown Sand and Desert Dunes* (Methuen, London, 1941).
 - [4] G. A. Loosmore and J. R. Hunt, Dust resuspension without saltation, *J. Geophys. Res.* **105**, 20663 (2000).
 - [5] Y. Shao, *Physics and Modelling of Wind Erosion* (Springer, Berlin, 2008).
 - [6] X. Zheng, *Mechanics of Wind-Blown Sand Movements* (Springer, Berlin, 2009).
 - [7] J. F. Kok, E. J. Parteli, T. I. Michaels, and D. B. Karam, The physics of wind-blown sand and dust, *Rep. Prog. Phys.* **75**, 106901 (2012).
 - [8] M. Klose and Y. Shao, Large-eddy simulation of turbulent dust emission, *Aeolian Res.* **8**, 49 (2013).
 - [9] W. Wu, G. Soligo, C. Marchioli, A. Soldati, and U. Piomelli, Particle resuspension by a periodically forced impinging jet, *J. Fluid Mech.* **820**, 284 (2017).
 - [10] D. Richter and M. Chamecki, Inertial effects on the vertical transport of suspended particles in a turbulent boundary layer, *Bound.-Lay. Meteorol.* **167**, 235 (2018).
 - [11] Y. Zhang, R. Hu, and X. Zheng, Large-scale coherent structures of suspended dust concentration in the neutral atmospheric surface layer: A large-eddy simulation study, *Phys. Fluids* **30**, 046601 (2018).
 - [12] T. Pätz, A. H. Clark, M. Valyrakis, and O. Durán, The physics of sediment transport initiation, cessation, and entrainment across aeolian and fluvial environments, *Rev. Geophys.* **58**, e2019RG000679 (2020).
 - [13] S. Rana, W. Anderson, and M. Day, An entrainment paradox: How hysteretic saltation and secondary transport augment atmospheric uptake of aeolian source materials, *J. Geophys. Res. Atmos.* **126**, e2020JD033493 (2021).

- [14] G. Ziskind, M. Fichman, and C. Gutfinger, Resuspension of particulates from surfaces to turbulent flows—review and analysis, *J. Aerosol Sci.* **26**, 613 (1995).
- [15] C. Henry and J. P. Minier, Progress in particle resuspension from rough surfaces by turbulent flows, *Prog. Energy Combust. Sci.* **45**, 1 (2014).
- [16] B. Nasr, G. Ahmadi, A. R. Ferro, and S. Dhaniyala, Overview of mechanistic particle resuspension models: Comparison with compilation of experimental data, *J. Adhes. Sci. Technol.* **33**, 2631 (2019).
- [17] Y. Kim, A. Gidwani, B. E. Wyslouzil, and C. W. Sohn, Source term models for fine particle resuspension from indoor surfaces, *Build. Environ.* **45**, 1854 (2010).
- [18] A. H. Ibrahim, P. F. Dunn, and R. M. Brach, Microparticle detachment from surfaces exposed to turbulent air flow: Controlled experiments and modeling, *J. Aerosol Sci.* **34**, 765 (2003).
- [19] M. W. Reeks, J. Reed, and D. Hall, On the resuspension of small particles by a turbulent flow, *J. Phys. D* **21**, 574 (1988).
- [20] M. W. Reeks and D. Hall, Kinetic models for particle resuspension in turbulent flows: Theory and measurement, *J. Aerosol Sci.* **32**, 1 (2001).
- [21] C. Henry and J. P. Minier, A stochastic approach for the simulation of particle resuspension from rough substrates: Model and numerical implementation, *J. Aerosol Sci.* **77**, 168 (2014).
- [22] C. Henry and J.-P. Minier, Colloidal particle resuspension: On the need for refined characterisation of surface roughness, *J. Aerosol Sci.* **118**, 1 (2018).
- [23] W. Anderson and C. Meneveau, Dynamic roughness model for large-eddy simulation of turbulent flow over multiscale, fractal-like rough surfaces, *J. Fluid Mech.* **679**, 288 (2011).
- [24] X. I. A. Yang and C. Meneveau, Modelling turbulent boundary layer flow over fractal-like multiscale terrain using large-eddy simulations and analytical tools, *Philos. Trans. R. Soc. A* **375**, 20160098 (2017).
- [25] M. M. Metzger and J. C. Klewicki, A comparative study of near-wall turbulence in high and low Reynolds number boundary layers, *Phys. Fluids* **13**, 692 (2001).
- [26] R. Örlü and P. Schlatter, On the fluctuating wall-shear stress in zero pressure-gradient turbulent boundary layer flows, *Phys. Fluids* **23**, 021704 (2011).
- [27] P. H. Alfredsson, R. Örlü, and P. Schlatter, The viscous sublayer revisited—exploiting self-similarity to determine the wall position and friction velocity, *Exp. Fluids* **51**, 271 (2011).
- [28] C. Meneveau and J. Katz, Scale-invariance and turbulence models for large-eddy simulation, *Annu. Rev. Fluid Mech.* **32**, 1 (2000).
- [29] S. B. Pope, *Turbulent Flows* (Cambridge University Press, Cambridge, 2000).
- [30] P. Sagaut, *Large Eddy Simulation for Incompressible Flows* (Springer, Berlin, 2001).
- [31] R. D. Moser, S. W. Haering, and G. R. Yalla, Statistical properties of subgrid-scale turbulence models, *Annu. Rev. Fluid Mech.* **53**, 255 (2021).
- [32] J. G. M. Kuerten, Point-particle DNS and LES of particle-laden turbulent flow—a state-of-the-art review, *Flow Turbul. Combust.* **97**, 689 (2016).
- [33] C. Marchioli, Large-eddy simulation of turbulent dispersed flows: A review of modelling approaches, *Acta Mech.* **228**, 741 (2017).
- [34] U. Piomelli and E. Balaras, Wall-layer models for large-eddy simulations, *Annu. Rev. Fluid Mech.* **34**, 349 (2002).
- [35] J. Larsson, S. Kawai, J. Bodart, and I. Bermejo-Moreno, Large eddy simulation with modeled wall-stress: Recent progress and future directions, *Mech. Eng. Rev.* **3**, 15 (2016).
- [36] S. T. Bose and G. I. Park, Wall-modeled large-eddy simulation for complex turbulent flows, *Annu. Rev. Fluid Mech.* **50**, 535 (2018).
- [37] P. L. Johnson, M. Bassenne, and P. Moin, Turbophoresis of small inertial particles: Theoretical considerations and application to wall-modelled large-eddy simulations, *J. Fluid Mech.* **883**, A27 (2020).
- [38] I. Marusic, R. Mathis, and N. Hutchins, Predictive model for wall-bounded turbulent flow, *Science* **329**, 193 (2010).
- [39] R. Mathis, N. Hutchins, and I. Marusic, A predictive inner-outer model for streamwise turbulence statistics in wall-bounded flows, *J. Fluid Mech.* **681**, 537 (2011).

- [40] M. Inoue, R. Mathis, I. Marusic, and D. I. Pullin, Inner-layer intensities for the flat-plate turbulent boundary layer combining a predictive wall-model with large-eddy simulations, *Phys. Fluids* **24**, 075102 (2012).
- [41] L. Agostini and M. A. Leschziner, Predicting the response of small-scale near-wall turbulence to large-scale outer motions, *Phys. Fluids* **28**, 015107 (2016).
- [42] G. Yin, W.-X. Huang, and C.-X. Xu, Prediction of near-wall turbulence using minimal flow unit, *J. Fluid Mech.* **841**, 654 (2018).
- [43] L. Wang, R. Hu, and X. Zheng, A scaling improved inner-outer decomposition of near-wall turbulent motions, *Phys. Fluids* **33**, 045120 (2021).
- [44] M. Yu and C.-X. Xu, Predictive models for near-wall velocity and temperature fluctuations in supersonic wall-bounded turbulence, *J. Fluid Mech.* **937**, A32 (2022).
- [45] M. O'Neill, A sphere in contact with a plane in a slow shear linear flow, *Chem. Eng. Sci.* **23**, 1293 (1968).
- [46] B. V. Derjaguin and L. Landau, Theory of the stability of strongly charged lyophobic sols and of the adhesion of strongly charged particles in solution of electrolytes, *Acta Physicochim. USSR* **14**, 633 (1941).
- [47] E. J. W. Verwey and J. T. G. Overbeek, *Theory of the Stability of Lyophobic Colloids* (Elsevier, New York, 1948).
- [48] C. Henry, J.-P. Minier, and G. Lefevre, Numerical study on the adhesion and reentrainment of nondeformable particles on surfaces: The role of surface roughness and electrostatic forces, *Langmuir* **28**, 438 (2012).
- [49] P. Diplas, C. L. Dancy, A. O. Celik, M. Valyrakis, K. Greer, and T. Akar, The role of impulse on the initiation of particle movement under turbulent flow conditions, *Science* **322**, 717 (2008).
- [50] A. O. Celik, P. Diplas, C. L. Dancy, and M. Valyrakis, Impulse and particle dislodgement under turbulent flow conditions, *Phys. Fluids* **22**, 046601 (2010).
- [51] H. Lee, M. Y. Ha, and S. Balachandar, Work-based criterion for particle motion and implication for turbulent bed-load transport, *Phys. Fluids* **24**, 116604 (2012).
- [52] H. Choi and P. Moin, Grid-point requirements for large eddy simulation: Chapman's estimates revisited, *Phys. Fluids* **24**, 011702 (2012).
- [53] X. I. A. Yang and K. P. Griffin, Grid-point and time-step requirements for direct numerical simulation and large-eddy simulation, *Phys. Fluids* **33**, 015108 (2021).
- [54] X. I. A. Yang, J. Hong, M. Lee, and X. L. D. Huang, Grid resolution requirement for resolving rare and high intensity wall-shear stress events in direct numerical simulations, *Phys. Rev. Fluids* **6**, 054603 (2021).
- [55] E. A. Matida, K. Nishino, and K. Torii, Statistical simulation of particle deposition on the wall from turbulent dispersed pipe flow, *Int. J. Heat Fluid Flow* **21**, 389 (2000).
- [56] S. S. Kumar, X. Huang, X. Yang, and J. Hong, Three dimensional flow motions in the viscous sublayer, *Theor. Appl. Mech. Lett.* **11**, 100239 (2021).
- [57] J. Graham, K. Kanov, X. I. A. Yang, M. Lee, N. Malaya, C. C. Lalescu, R. Burns, G. Eyink, A. Szalay, R. D. Moser, and C. Meneveau, A web services accessible database of turbulent channel flow and its use for testing a new integral wall model for LES, *J. Turbul.* **17**, 181 (2016).
- [58] P. L. Johnson and C. Meneveau, Predicting viscous-range velocity gradient dynamics in large-eddy simulations of turbulence, *J. Fluid Mech.* **837**, 80 (2018).
- [59] A. K. M. F. Hussain and W. C. Reynolds, Measurements in fully developed turbulent channel flow, *J. Fluids Eng.* **97**, 568 (1975).
- [60] J. Kim, P. Moin, and R. Moser, Turbulence statistics in fully developed channel flow at low Reynolds number, *J. Fluid Mech.* **177**, 133 (1987).
- [61] T. Tsukahara, Y. Seki, H. Kawamura, and D. Tochio, in *Proceedings of the Fourth International Symposium on Turbulence and Shear Flow Phenomena, Williamsburg*, edited by J. K. Eaton, R. Friedrich, T. B. Gatski, and J. A. C. Humphrey (Begell, Danbury, 2005), pp. 935–940.
- [62] R. Hu and X. Zheng, Energy contributions by inner and outer motions in turbulent channel flows, *Phys. Rev. Fluids* **3**, 084607 (2018).

- [63] A. Banari, C. Henry, R. H. Fank Eidt, P. Lorenz, K. Zimmer, U. Hampel, and G. Lecrivain, Evidence of collision-induced resuspension of microscopic particles from a monolayer deposit, *Phys. Rev. Fluids* **6**, L082301 (2021).
- [64] M. Lee and R. D. Moser, Direct numerical simulation of turbulent channel flow up to $Re_\tau \approx 5200$, *J. Fluid Mech.* **774**, 395 (2015).
- [65] LESGO code, available at <https://lesgo.me.jhu.edu/>.
- [66] F. Porté-Agel, C. Meneveau, and M. B. Parlange, A scale-dependent dynamic model for large-eddy simulation: Application to a neutral atmospheric boundary layer, *J. Fluid Mech.* **415**, 261 (2000).
- [67] E. Bou-Zeid, C. Meneveau, and M. Parlange, A scale-dependent Lagrangian dynamic model for large eddy simulation of complex turbulent flows, *Phys. Fluids* **17**, 025105 (2005).
- [68] C. H. Moeng, A large-eddy-simulation model for the study of planetary boundary-layer turbulence, *J. Atmos. Sci.* **41**, 2052 (1984).
- [69] R. Hu, P. L. Johnson, and C. Meneveau, Eleventh International Symposium on Turbulence and Shear Flow Phenomena (TSFP11), Southampton, 2019 (unpublished).
- [70] A. D. Bragg, D. H. Richter, and G. Wang, Settling strongly modifies particle concentrations in wall-bounded turbulent flows even when the settling parameter is asymptotically small, *Phys. Rev. Fluids* **6**, 124301 (2021).
- [71] H. Brenner, The slow motion of a sphere through a viscous fluid towards a plane surface, *Chem. Eng. Sci.* **16**, 242 (1961).
- [72] R. G. Cox and H. Brenner, The slow motion of a sphere through a viscous fluid towards a plane surface—II Small gap widths, including inertial effects, *Chem. Eng. Sci.* **22**, 1753 (1967).
- [73] M. D. A. Cooley and M. E. O’Neill, On the slow motion generated in a viscous fluid by the approach of a sphere to a plane wall or stationary sphere, *Mathematika* **16**, 37 (1969).
- [74] W.-P. Breugem, in *Proceedings of the ASME 2010 3rd Joint US-European Fluids Engineering Summer Meeting collocated with 8th International Conference on Nanochannels, Microchannels, and Minichannels. ASME 2010 3rd Joint US-European Fluids Engineering Summer Meeting: Volume 1, Symposia-Parts A, B, and C, Montreal, 2010* (ASME, New York, 2010), paper FEDSM-ICNMM2010-30634, pp. 2381–2392.
- [75] T. Kempe and J. Fröhlich, Collision modelling for the interface-resolved simulation of spherical particles in viscous fluids, *J. Fluid Mech.* **709**, 445 (2012).
- [76] J. A. Simeonov and J. Calantoni, Modeling mechanical contact and lubrication in direct numerical simulations of colliding particles, *Int. J. Multiph. Flow* **46**, 38 (2012).
- [77] E. Izard, T. Bonometti, and L. Lacaze, Modelling the dynamics of a sphere approaching and bouncing on a wall in a viscous fluid, *J. Fluid Mech.* **747**, 422 (2014).
- [78] P. Costa, B. J. Boersma, J. Westerweel, and W.-P. Breugem, Collision model for fully resolved simulations of flows laden with finite-size particles, *Phys. Rev. E* **92**, 053012 (2015).
- [79] E. Biegert, B. Vowinkel, and E. Meiburg, A collision model for grain-resolving simulations of flows over dense, mobile, polydisperse granular sediment beds, *J. Comput. Phys.* **340**, 105 (2017).
- [80] R. Jain, S. Tschisgale, and J. Fröhlich, A collision model for DNS with ellipsoidal particles in viscous fluid, *Int. J. Multiph. Flow* **120**, 103087 (2019).
- [81] C. Rettinger and U. Rüde, An efficient four-way coupled lattice Boltzmann–discrete element method for fully resolved simulations of particle-laden flows, *J. Comput. Phys.* **453**, 110942 (2022).
- [82] T. M. Nijssen, M. Ottens, and J. T. Padding, A note on the modelling of lubrication forces in unresolved simulations, *Powder Technol.* **413**, 118017 (2023).
- [83] Z. Zhu, R. Hu, and X. Zheng, A multiple-time-step integration algorithm for particle-resolved simulation with physical collision time, [arXiv:2207.13969](https://arxiv.org/abs/2207.13969) (2022).
- [84] D. J. Jeffrey and Y. Onishi, Calculation of the resistance and mobility functions for two unequal rigid spheres in low-Reynolds-number flow, *J. Fluid Mech.* **139**, 261 (1984).
- [85] S. Elghobashi, On predicting particle-laden turbulent flows, *Appl. Sci. Res.* **52**, 309 (1994).